PAPER

Thermal analysis of micropolar hybrid nanofluid inspired by 3D stretchable surface in porous media

Aisha M. Alqahtani,[a] Basharat Ullah,[b] Bilal Ahmad,[c] Umar Khan, [ID] *[c] Hafiz Abdul Wahab[c] and Roobaea Alroobaea [ID] [d]

Applications: the study of highly advanced hybrid nanofluids has aroused the interest of academics and engineers, particularly those working in the fields of chemical and applied thermal engineering. The improved properties of hybrid nanoliquids are superior to those of earlier classes of nanofluids (which are simply referred to as nanofluids). Therefore, it is essential to report on the process of analyzing nanofluids by passing them through elastic surfaces, as this is a typical practice in engineering and industrial applications. *Purpose and methodology*: the investigation of hybrid nanoliquids was the sole focus of this research, which was conducted using a stretched sheet. Using supporting correlations, an estimate was made of the improved thermal conductivity, density, heat capacitance, and viscosity. In addition, the distinctiveness of the model was increased by the incorporation of a variety of distinct physical limitations, such as thermal slip, radiation, micropolarity, uniform surface convection, and stretching effects. After that, a numerical analysis of the model was performed, and the physical results are presented. *Core findings*: the results of the model showed that it is possible to attain the desired momentum of hybrid nanofluids by keeping the fluidic system at a uniform suction, and that this momentum may be enhanced by increasing the force of the injecting fluid *via* a stretched sheet. Surface convection, thermal radiation, and high dissipative energy are all great physical instruments that can be used to acquire heat in hybrid nanofluids. This heat acquisition is significant from both an applied thermal engineering perspective and a chemical engineering perspective. The features of simple nano and common hybrid nanoliquids have been compared and the results indicate that hybrid nanofluids exhibit dominant behavior when measured against the percentage concentration of nanoparticles, which enables them to be used in large-scale practical applications.

Introduction

Heat-converted fluids in mixtures such as ethylene glycol, water and oil with low thermal conductivity are essential materials in the development of a thermal scheme. To further increase their properties, plentiful research has been carried out into the thermal conveyance features of these fluids. Latiff *et al.* [1] studied a nanometer solid component in a liquid, which remained a state-of-the-art result, but the unsuitable liquid used meant a breakthrough in technological development and industrial scale was not achieved. The nanoparticle increase the thermal conductivity as good heat transfer fluids, inside or outside the boundaries.

aDepartment of Mathematical Sciences, College of Science, Princess Nourah Bint Abdulrahman University, P.O. Box 84428, Riyadh 11671, Saudi Arabia

bDepartment of Mathematics, Mohi-ud-Din Islamic University, Nerian Sharif, AJ&K, Pakistan

cDepartment of Mathematics and Statistics, Hazara University, Mansehra, Pakistan. E-mail: umar_jadoon4@yahoo.com

dDepartment of Computer Science, College of Computers and Information Technology, Taif University, P.O. Box 11099, Taif 21944, Saudi Arabia

Because of the high thermal conductivity of better nano-fluids, many physicists and researchers are engaged in studying emerging thermal arrangements and processes, which are useful for industrial processes which use nanofluids. By adding Al_2O_3, SiO_3 and TiO_2, Khan *et al.* [2] investigated how the thermal conductivity changes in water. Amirsom *et al.* [3] studied heat flow in previous nanofluids made from linearly extended plates. The heat generation process and fascinating properties of nano-fluids, which are exponentially strained in one direction, was first studied by Adnan *et al.* [4] who analyzed the unsteady flow of MHD which is a dusty nanofluid, which was first examined by Ullah *et al.* [5] who analyzed the effect of a biochemical reaction on the MHD stream of a nanofluid, which was discovered by Murtaza *et al.* [6] to be an exponentially expanded surface.

Because of its importance to numerous fields of study, the flow field and heat transfer properties within a porous medium have received extensive attention from academics. In fluid mechanics, the behavior of a fluid as it streams past a porous medium is described by the term "fluid flow past a porous medium." While some of the fluid moves through the medium, a greater concentration of the fluid fills the pores of the porous

Paper

medium; for instance, flow through a sponge or wood, or percolation of water through sand or another porous medium. Flows of oil, gas, and water inside oil reservoirs, insulation engineering, geo-mechanisms (such as geothermal reservoirs), and increased oil recovery are all examples of issues related to porous media. In addition to their obvious usefulness in preventing the detrimental effects of free natural convection on a stretched surface, porous media are also crucial in a number of other ways. Raptis[7] investigated the flow of micropolar fluids in porous media under the assumption of a boundary layer. The authors Ferdows et al.[8] investigated the effect of an exponentially stretched sheet on the flow of a mixed convective magneto hydrodynamic nanofluid across a porous medium. To better understand how a micropolar fluid reacts when a sheet is stretched across a porous medium, Ullah et al.[9] recently conducted research in this area. Adnan[10] studied all the types of nanofluids, which is very useful. Tuz et al.[11] carried out a detailed study of nanofluids. As nanoparticles have very small size, optimal effectiveness and permanency in technical and different biomedical ground have not been yet cleared.

The plethora of applications of rotating flows in geological physics and engineering, such as the movement of magma within the earth's mantle, the extension of tectonic plates beneath a rotating ocean, anticyclonic flow revolutions, the centrifugal percolation process, the processing of chemicals and foods, rotating machinery, and the dynamics of tornadoes and hurricanes, are the driving force behind the study of such flows. The concept of flow near a stretched sheet immersed in a rotating fluid was first proposed by Rehman.[12] This article defines a parameter which represents the ratio between the rotational velocity and the stretching velocity of the sheet. The effects of rotation across an exponentially stretched region on the behavior of a nanofluid were quantitatively investigated by Mishra et al.[13] Khan et al.[14] performed a comparative study on the impact of rotation on a nanofluid due to a convectively heated plate but which was also stretched exponentially.

Uddin et al.[15] studied how to improve the biochemical automatic (CMP) for which they established the CMP of silver (Ag) which helps in making high-presentation strategies of graphene and microelectronics. Zhang et al.[16] showed that in titanium alloys the nanoparticles play a significant role for the action of CMP for a process in which the nanospheres are heated. Nanofluids have attached significant attention in heat transport bids because of their practical importance, that can be changed with the type of nanoparticle used in base fluid.

To improve the properties of nanofluids, which is concerning heat transfer experts, a new type of fluid has been developed, which is known as a hybrid nanofluid. Mixed nanofluids are made of two or more different nanoparticles using this method. The main purpose of hybrid nanofluid synthetization is to enhance nanofluid properties. Suresh et al.[17] undertook a comprehensive investigation into the synthesis of nanoparticle composites of copper and aluminum oxide. The hybrid nanofluid (Ag-Fe_2O_3) water procides with effective heat tranfer capacity as compared to the Fe_2O_3 water nanofluid. A comparison of the effects in previous work shows a good relationship. The effects show reductions in the velocity distribution with an increase in attractive parameters, whereas the distributions of temperature and application increase. Recently, many researchers[18,19] have reviewed the flow theory of micropolar fluids.

After reviewing the state of the art in the field of micropolar nanofluids, we came to the conclusion that the behavior of the flow of the three-dimensional boundary layer of a micropolar

Table 1 Thermo-physical properties of hybrid nanofluids and nanoparticles

Thermo-physical properties	ρ (kg m^{-3})	C_p (J kg^{-1}) K	k (kW mK^{-1})
Ethylene glycol–water	997.1	4179	0.613
Ag	8933	385	400
Fe_3O_4	4250	686.2	8.9538

Table 2 Comparison of the x- and y-direction skin friction coefficients for nanofluids and hybrid nanofluids as a function of the vortex viscosity (R_1), rotation angle (ε), stretching angle (λ), porosity parameter (k_p), and nanoparticle volume fraction (ϕ)

R_1	ε	λ	k_p	ϕ	$\dfrac{-1}{(1-\phi_1)^{2.5}}f''(0)$	$\dfrac{(1-\phi_2)^{-2.5}}{(1-\phi_1)^{2.5}}f''(0)$	$\dfrac{-1}{(1-\phi_1)^{2.5}}g''(0)$	$\dfrac{(1-\phi_2)^{-2.5}}{(1-\phi_1)^{2.5}}g''(0)$
0.1	0.3	0.2	05	0.05	0.14788	0.56723	0.04579	0.34756
0.2					0.23876	0.72348	0.19837	0.37921
0.3					0.28743	1.73927	0.23764	0.67391
0.1	0.3	0.2	0.5	0.05	1.01257	1.03458	0.98357	0.83579
	0.5				1.12987	1.78934	0.48201	0.73946
	0.7				1.93476	1.87943	0.38197	0.39273
0.1	0.5	0.5	0.5	0.05	2.12874	2.78365	1.84646	1.89364
		1.0			2.48298	2.19748	1.78326	1.67420
		1.5			2.83933	2.47291	1.83467	1.73829
0.1	0.5	0.5	0.5	0.05	2.34560	2.48297	1.48349	1.48457
			1.0		2.75839	2.46389	1.56392	1.47344
			1.5		2.57389	2.67392	1.12489	1.23458
0.1	0.5	0.5	0.5	0.01	1.43492	1.56329	0.62784	0.47239
				0.05	1.63783	1.72934	0.57382	0.67238
				0.09	1.74937	1.47928	0.47398	0.46228

Table 3 Comparison of the x- and y-direction Nusselt numbers for nanofluids and hybrid nanofluids as a function of the vortex viscosity (R_1), rotation angle (ε), stretching angle ($-\lambda$), porosity parameter (k_p), and nanoparticle volume fraction (ϕ)

R_1	ε	λ	k_p	ϕ	$\frac{-k_{nf}}{k_f}\theta'(0)$	$\frac{-k_{hnf}}{k_f}\theta'(0)$
0.1	0.3	0.2	05	0.05	1.34668	2.98566
0.2					1.46654	2.45383
0.3					1.45579	2.45682
0.1	0.3	0.2	0.5	0.05	2.79344	1.85680
	0.5				2.45696	1.23569
	0.7				2.45987	1.43529
0.1	0.5	0.5	0.5	0.05	2.47498	1.75843
		1.0			2.76849	1.25478
		1.5			2.75647	1.74824
0.1	0.5	0.5	0.5	0.05	2.75839	1.73877
			1.0		2.48298	1.48290
			1.5		2.27484	1.72840
0.1	0.5	0.5	0.5	0.01	2.74833	1.36489
				0.05	2.34789	1.65748
				0.09	2.84947	1.73837

hybrid nanofluid in the presence of an exponentially stretched surface had not yet been investigated. The effects on the flow of porous media and rotation have been analyzed in detail. In this study, a micropolar hybrid nanofluid is compared to a simple micropolar nanofluid. Dimensionless velocities, microrotation, and temperature profiles are shown as functions of these and other physical parameters in Tables 1–3.

Description of the problem

An exponentially stretched surface embedded in a porous medium initiates the incompressible, rotary flow of a hybrid nanofluid in terms of micropolar theory. The influence of thermal radiation on channel flow is also considered. Each tube wall has different characteristics. The bottom wall of the channel has coordinates along the objective lens x, and the velocity is $U_w = U_0\, e^{\frac{x+y}{L}}$, in a stretched state. The wall velocity equation along the target direction y is equal to $V_w = V_0\, e^{\frac{x+y}{L}}$. It is assumed that the height of the channel can be changed by moving the upper wall and closing the lower wall. The flow is limited to the zone $z > 0$, and the stretched surface lies in the plane $z = 0$. The nanofluid rotates around the vertical objective lens z at a constant angular velocity Ω. Fig. 1 clearly illustrates the expressions given above.

Based on the following assumptions, the fluid is considered to be a mixture of three components.

(1) The fluid is not compressible.
(2) The reaction is non-chemical.
(3) Viscosity dissipation is negligible.
(4) The particles are in thermal equilibrium.

Governing equations

In the previous hypothesis, the basic equations of continuity, moment, micropolarity, and energy can be written in dimensional form see ref. 20.

$$\frac{\partial u}{\partial x} + \frac{\partial v}{\partial y} + \frac{\partial w}{\partial z} = 0, \tag{1}$$

$$u\frac{\partial u}{\partial x} + v\frac{\partial u}{\partial y} + w\frac{\partial u}{\partial z} - 2\Omega v = \left(\frac{\mu_{hnf+k}}{\rho_{hnf}}\right)\frac{\partial^2 u}{\partial z^2} - \frac{k}{\rho_{hnf}}\left(\frac{\partial N_2}{\partial z}\right) - \frac{\nu_{hnf}u}{K^*}, \tag{2}$$

$$u\frac{\partial v}{\partial x} + v\frac{\partial v}{\partial y} + w\frac{\partial v}{\partial z} + 2\Omega u = \left(\frac{\mu_{hnf+k}}{\rho_{hnf}}\right)\frac{\partial^2 v}{\partial z^2} + \frac{k}{\rho_{hnf}}\left(\frac{\partial N_1}{\partial z}\right) - \frac{\nu_{hnf}v}{K^*}, \tag{3}$$
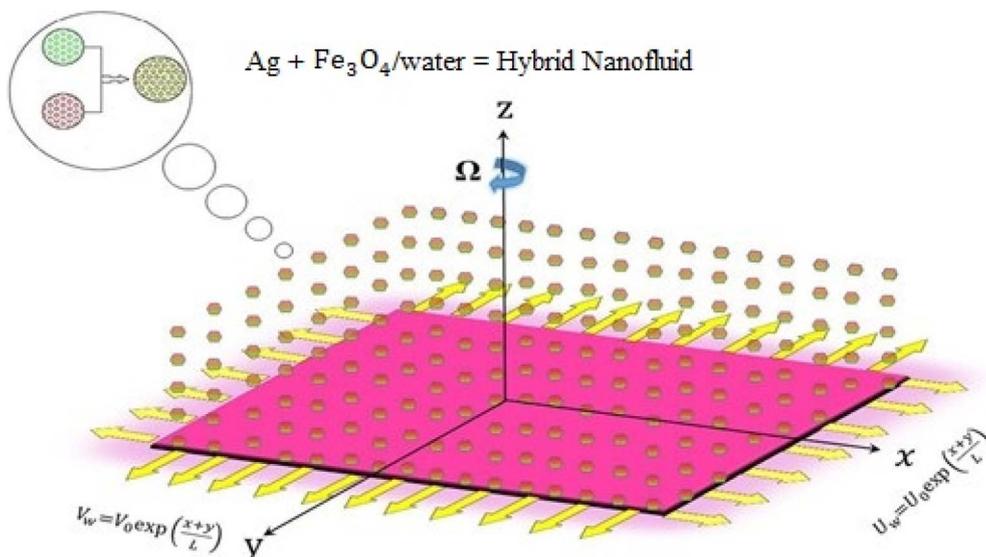

Fig. 1 Geometry of the problem.

$$\rho_{hnf} j \left[u \frac{\partial N_1}{\partial x} + v \frac{\partial N_1}{\partial y} + w \frac{\partial N_1}{\partial z} \right] = \chi_{hnf} \frac{\partial^2 N_1}{\partial z^2} - 2kN_1 - k \frac{\partial v}{\partial z}, \quad (4)$$

$$\rho_{hnf} j \left[u \frac{\partial N_1}{\partial x} + v \frac{\partial N_1}{\partial y} + w \frac{\partial N_1}{\partial z} \right] = \chi_{hnf} \frac{\partial^2 N_1}{\partial z^2} - 2kN_1 - k \frac{\partial v}{\partial z}, \quad (5)$$

$$\frac{\partial T}{\partial x} + v \frac{\partial T}{\partial y} + w \frac{\partial T}{\partial z} = \alpha_{hnf} \left(\frac{\partial^2 T}{\partial z^2} \right). \quad (6)$$

The boundary conditions of the problem are now discussed. Here the components are u and v of the velocity along the x and y directions, respectively. Furthermore, μ_{hnf} represents the effective dynamic viscosity of a hybrid nanofluid; the effective density of a hybrid nanofluid is represented by ρ_{hnf}; $(\rho c_p)_{nf}$ is heat capacity; k_{hnf} represents the thermal conductivity of the hybrid nanofluid ; σ_{hnf} is the electrical conductivity; B is the imposed magnetic field for the fluid and k is the mean absorption coefficient. The boundary conditions in the considered problem are:

$$u = U_w, \quad v = V_w, \quad T = T_w, \quad N_1 = n\frac{\partial v}{\partial z}, \quad N_2 = -n\frac{\partial u}{\partial z} \quad \text{at } z = 0$$

$$u \to \infty, \quad v \to 0, \quad T \to T_\infty, \quad N_1 \to 0, \quad N_2 \to 0 \quad \text{as } z \to \infty, \quad (7)$$

where U_w, V_w and T_w are the velocities and temperature at the wall as:

$$U_w = U_0 e^{\frac{x+y}{L}}, \quad V_w = V_0 e^{\frac{x+y}{L}}, \quad T_w = T_\infty + T_0 e^{\frac{B(x+y)}{2L}}. \quad (8)$$

Here N_1 and N_2 are the angular velocity and u and v are the velocities along the x, y and z-axes; T_w represents the temperature of the stretched sheet; T_∞ represents the temperature without stretching; L is the reference length; U_0, V_0 and T_0 are constant; B is the heat index; n is the edge limit whose interval is $0 \le n \le 1$. If $n = 0$, it means that there are many microelements ending the outward stretching and these microelements cannot be rotated. If $n = 0.5$, it means that there are trace elements, and if $n = 1$, it means boundary layer turbulence.

The similarity transformations are listed below:

$$u = U_0 e^{\frac{x+y}{L}} f'(\eta), \quad v = U_0 e^{\frac{x+y}{L}} g'(\eta),$$

$$w = -\left(\frac{\nu U_0}{2L} \right)^{\frac{1}{2}} e^{\frac{x+y}{2L}} [f(\eta) + \eta f'(\eta) + g + \eta g'(\eta)], \quad N_1$$

$$= \frac{U_0}{2\nu L} (2U_0 \nu L)^{\frac{1}{2}} e^{3\left(\frac{x+y}{2L}\right)} h_1(\eta), \quad N_2$$

$$= \frac{U_0}{2\nu L} (\nu L 2U_0)^{\frac{1}{2}} e^{3\left(\frac{x+y}{2L}\right)} h_2(\eta), \quad T = T_\infty + T_0 e^{\frac{B(x+y)}{2L}} \theta(\eta), \quad \eta$$

$$= \left(\frac{U_0}{2\nu L} \right)^{\frac{1}{2}} e^{\frac{x+y}{2L}} z. \quad (9)$$

Using eqn (9) in eqn (1)–(6), the continuity equation can be satisfied, and the momentum, microrotation, and energy equations can be simplified to the following forms:

$$\frac{\rho_f}{\rho_{hnf}} (A(\phi) + R_1) f'''(\eta) + f''(\eta)(f(\eta) + g(\eta))$$

$$-2f'(\eta)(f'(\eta) + g'(\eta)) - \frac{\rho_f}{\rho_{hnf}} R_1 h'_2(\eta) - \frac{\nu_{hnf}}{\nu_f} k_p f'(\eta) + 4\varepsilon g'(\eta) = 0, \quad (10)$$

$$\frac{\rho_f}{\rho_{hnf}} (A(\phi) + R_1) g'''(\eta) + g''(\eta)(f(\eta) + g(\eta)) - 2g'(\eta)(f'(\eta) + g'(\eta))$$

$$+ \frac{\rho_f}{\rho_{hnf}} R_1 h'_1(\eta) - \frac{\nu_{hnf}}{\nu_f} K_p g'(\eta) - 4\varepsilon f'(\eta) = 0, \quad (11)$$

$$\frac{\rho_f}{\rho_{hnf}} R_2 h''_1(\eta) - R_1 R_3 (2h_1(\eta) + g''(\eta)) - 3 h_1(\eta)(f'(\eta) + g'(\eta))$$

$$+ h'_1(\eta)(f(\eta) + g(\eta)) = 0, \quad (12)$$

$$\frac{\rho_f}{\rho_{hnf}} R_2 h''_2(\eta) - R_1 R_3 (2h_2(\eta) - f''(\eta)) - 3h_2(\eta)(f'(\eta) + g'(\eta))$$

$$+ f'(\eta) + g'(\eta) h'_2(\eta)(f(\eta) + g(\eta)) = 0, \quad (13)$$

$$\frac{1}{\Pr} \frac{k_{hnf}}{k_f} \frac{1}{\left\{ (1 - \phi_2) \left[(1 - \phi_1) + \phi_1 \frac{(\rho C_p)_{s1}}{(\rho C_p)_f} \right] \right\} + \phi_2 \frac{(\rho C_p)_{s2}}{(\rho C_p)_f}} \theta''(\eta)$$

$$- B(f'(\eta) + g'(\eta))\theta(\eta) + (f(\eta) + g(\eta))\theta'(\eta)$$

$$= 0. \quad (14)$$

In the same way, similarity transformation (9) can be used to reduce the boundary condition to:

$$f(0) = 0, f'(0) = 1, g(0) = 0, g'(0) = \lambda, \theta(0) = 1, h_1(0) = ng''(0), h_2(0) = -ng''(0), \text{ as } \eta \to 0, f' \to 0, g' \to 0, \theta \to 0, h_1 \to 0, h_2 \to 0 \text{ as } \eta \to \infty. \quad (15)$$

where $R_1, R_2, R_3, k_p, \Pr$ and ε are the different parameters. These parameters can be expressed mathematically:

$$R_1 = \frac{k}{\mu}, \quad R_2 = \frac{\chi_{hnf}}{\mu j}, \quad R_3 = \frac{2\nu L}{jU_w}, \quad k_p = \frac{2\nu L}{K^* U_w},$$

$$\Pr = \frac{(\mu C_p)_f}{k_f}, \quad \lambda = \frac{V_0}{U_0}, \quad \varepsilon = \frac{\Omega_0 L}{U_0}, \quad \text{and} A(\phi)$$

$$= \frac{\mu_{hnf}}{\mu_f} \frac{1}{(1 - \phi_1)^{2.5}(1 - \phi_2)^{2.5}}. \quad (16)$$

Moreover, μ_{hnf}, ρ_{hnf}, $(\rho c_p)_{hnf}$, k_{hnf}, χ_{hnf} and α_{hnf} can be expressed mathematically as:

$$\rho_{hnf} = \{(1 - \phi_1)[(1 - \phi_2)\rho_f + \phi_1 \rho_{s1}]\} + \phi_2 \rho_{s2}, \quad (17)$$

$$\mu_{hnf} = \frac{\mu_f}{(1 - \phi_2)^{5/2}(1 - \phi_1)^{5/2}}, \quad (18)$$

$$(\rho C_{\mathrm{p}})_{hnf} = [(1 - \phi_2)[(1 - \phi_1)(\rho C_{\mathrm{p}})_f + \phi_1(\rho C_{\mathrm{p}})_{s1}]] + \phi_2(\rho C_{\mathrm{p}})_{s2}, \quad (19)$$

$$k_{hnf} = k_{bf}\left[\frac{(k_{s_2} + 2k_{bf}) - 2\phi_2(k_{bf} - k_{s_2})}{(k_{s_2} + 2k_{bf}) + \phi_2(k_{bf} - k_{s_2})}\right], \quad (20)$$

$$k_{bf} = k_{\mathrm{f}}\left[\frac{(k_{s_1} + 2k_{\mathrm{f}}) - 2\phi_1(k_{\mathrm{f}} - k_{s_1})}{(k_{s_1} + 2k_{\mathrm{f}}) + \phi_1(k_{\mathrm{f}} - k_{s_1})}\right],$$

$$\chi_{hnf} = \left(\mu_{hnf} + \frac{k}{2}\right), \quad j, \quad j = \frac{2\nu L}{U_{\mathrm{w}}} \quad (21)$$

$$\alpha_{hnf} = \frac{k_{hnf}}{(\rho c_{\mathrm{p}})_{hnf}}. \quad (22)$$

where k_{s_1} and k_{s_2} are the thermal conductivities of the nanoparticles. In the above formulae ϕ_1 and ϕ_2 are the fixed volume fractions of ferric oxide (Fe_3O_4) and silver (Ag), where ρ_{s_1} is ferric oxide Fe_3O_4 and impurities. The chemical density of nanoparticles is ρ_{s_2}, which is the density of hybrid ethylene glycol nanoparticles.

The equations are reduced from higher order to first order by the shooting method and then the problem is solved by using the R–K–4 method (coupled with the shooting technique).

Procedure for solution

Solve the nonlinear ordinary differential equations on the right. Under conditions (10)–(14) and limits (15), this can be solved mathematically. To apply the photographic method, the Runge–Kutta method is used to convert the high-order ODE to the first-order ODE to obtain the exact solution of the equation. For graphical analysis, we use mathematical software called Mathematica. In this conversion, we can write:

$$x_1 = f(\eta), \ x_2 = f'(\eta), \ x_3 = f''(\eta), \ x_4 = f'''(\eta),$$

$$x_5 = g(\eta), \ x_6 = g'(\eta), \ x_7 = g''(\eta), \ x_8 = g'''(\eta),$$

$$x_9 = h_1(\eta), \quad x_{10} = h'_1(\eta), \quad x_{11} = h''_1(\eta),$$

$$x_{12} = h_2(\eta), \quad x_{13} = h'_2(\eta), \quad x_{14} = h''_2(\eta),$$

$$x_5 = \theta(\eta), \ x_{16} = \theta'(\eta), \ x_{17} = \theta''(\eta),$$

$$x'_1 = f'(\eta) = x_2,$$

$$x'_2 = f''(\eta) = x_3,$$

$$x'_3 = f'''(\eta) = x_4,$$

$$x'_5 = g'(\eta) = x_6,$$

$$x'_6 = g''(\eta) = x_7,$$

$$x'_7 = g'''(\eta) = x_8,$$

$$x'_9 = h'_1(\eta) = x_{10},$$

$$x'_{10} = h''_1(\eta) = x_{11},$$

$$x'_{12} = h'_2(\eta) = x_{13},$$

$$x'_{13} = h''_2(\eta) = x_{14},$$

$$x'_{15} = \theta'(\eta) = x_{16},$$

$$x'_{16} = \theta''(\eta) = x_{17}.$$

$$x'_3 = \frac{\rho_{hnf}}{\rho_{\mathrm{f}}(A(\phi) + R_1)}\left[2x_2(x_2 + x_6) + \frac{\rho_{\mathrm{f}}}{\rho_{hnf}}R_1 x_{13} + \frac{\nu_{hnf}}{\nu_{\mathrm{f}}}k_{\mathrm{p}}x_2 - x_3(x_1 + x_5) - 4\varepsilon x_6\right]. \quad (23)$$

$$x'_7 = \frac{\rho_{hnf}}{\rho_{\mathrm{f}}(A(\phi) + R_1)}\left[2x_6(x_2 + x_6) - \frac{\rho_{\mathrm{f}}}{\rho_{hnf}}R_1 x_{10} + \frac{\nu_{hnf}}{\nu_{\mathrm{f}}}k_{\mathrm{p}}x_6 - x_7(x_1 + x_5) + 4\varepsilon x_2\right]. \quad (24)$$

$$x'_{10} = \frac{\rho_{hnf}}{\rho_{\mathrm{f}}R_2}[R_1 R_3(2x_9 + x_7) + 3x_9(x_2 + x_6) - x_{10}(x_1 + x_5)]. \quad (25)$$

$$x'_{13} = \frac{\rho_{hnf}}{\rho_{\mathrm{f}}R_2}[R_1 R_3(2x_{12} - x_3) + 3x_{12}(x_2 + x_6) - x_{13}]. \quad (26)$$

$$x'_{17} = \mathrm{Pr}\frac{k_{\mathrm{f}}}{k_{hnf}}\left[\left\{(1 - \phi_2)\left[(1 - \phi_1) + \phi_1\frac{(\rho C_{\mathrm{p}})_{s1}}{(\rho C_{\mathrm{p}})_f}\right]\right\} + \phi_2\frac{(\rho C_{\mathrm{p}})_{s2}}{(\rho C_{\mathrm{p}})_f}\right]$$
$$\times [B(x_2 + x_6)x_{15} - (x_1 + x_5)x_{16}]. \quad (27)$$

Similarly, the boundary conditions are:

$$x_1(0) = 0, \ x_2(0) = 1, \ x_5(0) = 0, \ x_6(0) = \lambda, \ x_{15}(0) = 1,$$

$$x_9(0) = nx_7(0), \ x_{12}(0) = -nx_7(0), \text{ as } \eta \to 0,$$

$$x_2 \to 0, \ x_6 \to 0, \ x_{15} \to 0, \ x_9 \to 0, \ x_{12} \to 0 \text{ as } \eta \to \infty. \quad (28)$$

Paper

Interpretation of the results

In this section, our focus is on the analysis of fluid velocity and temperature under the impact of various parameters. Table 1 gives the thermo-physical properties of nanofluids. Several figures show the effect of the volume parameters in light of "volume" parameters that we will define. The mixed nano-particles the volume proportion of "nanoparticles" of ferric oxide Fe_3O_4 changes.

Stretched sheet velocity profiles

Fig. 2 and 3 show a study of the velocity distributions $f'(\eta)$ and $g'(\eta)$ in the x and y directions, showing simple water-based fluids, nanofluids (Ag/water) and mixed nanofluids Ag-Fe_3O_4/water. Fig. 2 and 3 graphically show changes in heat transfer and flow behavior affected by several new parameters. Fig. 2 and 3 explain the speed difference, where the value of the reduction of the change in the variable ε reflects a monotonous change. The only variation that can be observed is that the velocity of the hybrid nanofluid is slower than that of the pure nanofluid. This is mainly due to the high-density value of nanofluids which cannot be obtained. Fig. 3 defines the e of ε on velocity
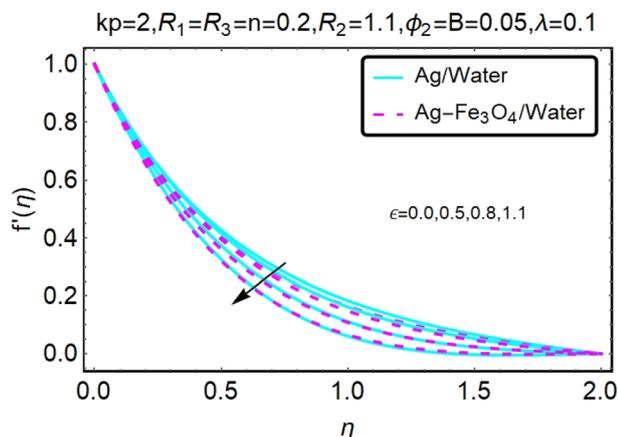
Fig. 2 Change in velocity profile by varying ε.
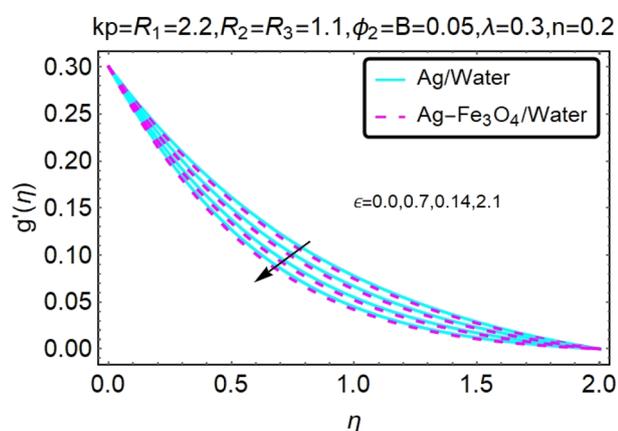
Fig. 3 Change in velocity profile by varying ε.
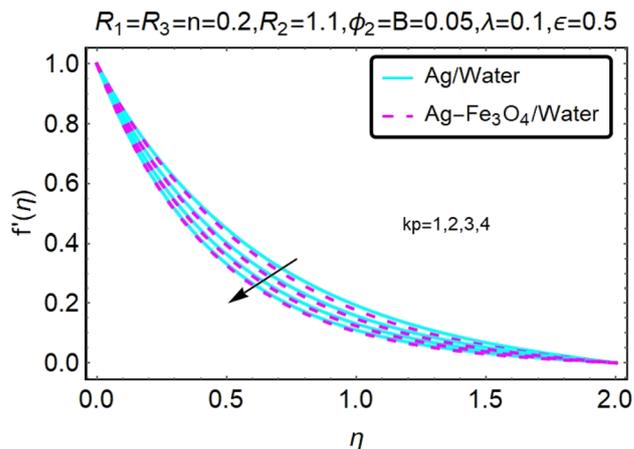
Fig. 4 Change in velocity profile by varying k_p.

circulation. The change in speed is also irrelevant. For mixed nanofluids, the low-speed principle is determined similarly.

Fig. 4 and 5 show the behavior of the velocity distribution $f'(\eta)$ and $g'(\eta)$ in the x and y directions, showing simple water-based fluids, nanofluids (Ag/water) and mixed nanofluids Ag-Fe_3O_4/water. Fig. 4 and 5 show the relationship between the conductivity of the velocity distribution and the porosity parameter k_p, and the comparison between nanofluid (Ag/water) and mixed nanofluid Ag-Fe_3O_4/water. The increase in the porosity parameter k_p causes the speed to decrease, due to the fact that the increase in porosity is inversely proportional to the permeability, so that the permeability decreases, which makes fluid flow more difficult and therefore both the speeds become slower.

Fig. 6 and 7 show a study of the velocity distribution $f'(\eta)$ and $g'(\eta)$ in the x and y directions, showing simple water-based fluids, nanofluids (Ag/water) and mixed nanofluids Ag-Fe_3O_4/water. In this section, the velocity distribution coefficient is shown when a turn occurs. These graphs are designed to calculate flow performance based on parameters. Therefore, Fig. 6 and 7 show that reducing the value of ϕ_2 will also reduce the velocity distribution.
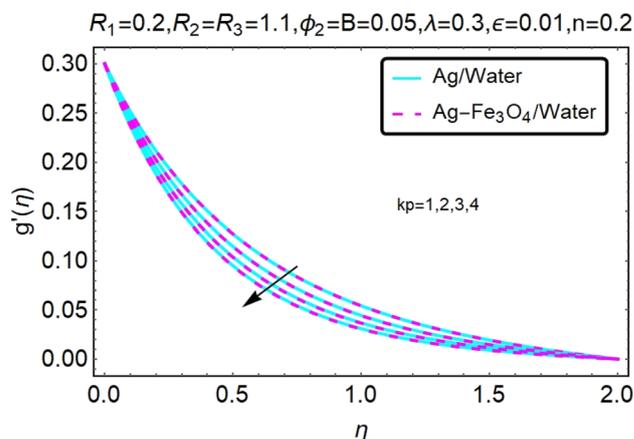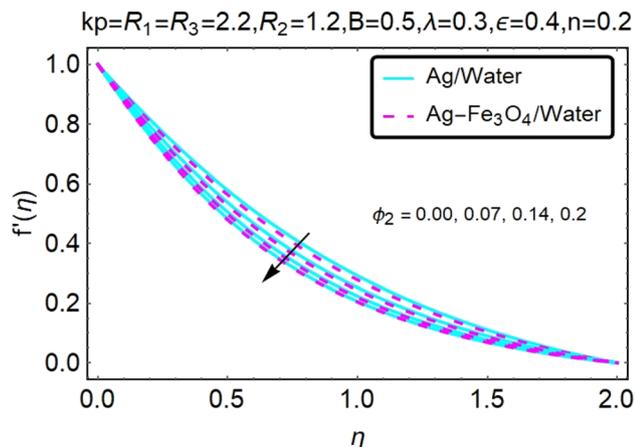

Fig. 5 Change in velocity profile by varying k_p.
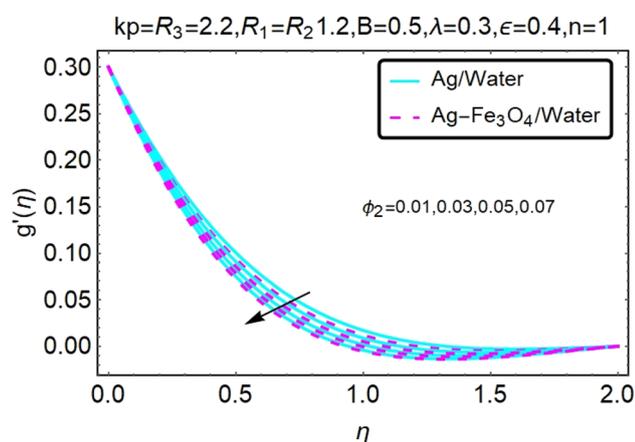
Fig. 6 Change in velocity profile by varying ϕ_2.

Fig. 7 Change in velocity profile by varying ϕ_2.

Fig. 8 and 9 show a study of the velocity distribution $f'(\eta)$ and $g'(\eta)$ in the x and y directions, showing simple water-based fluids, nanofluids (Ag/water) and mixed nanofluids Ag-Fe$_3$O$_4$/water. The related speed of nanofluids is slower than that of water and copper nanofluids. In this section, we discuss the
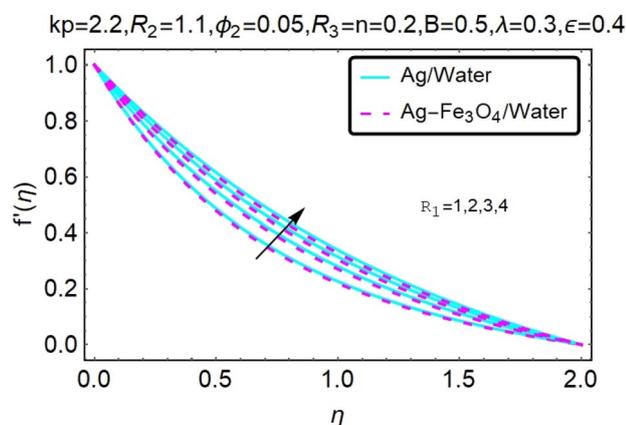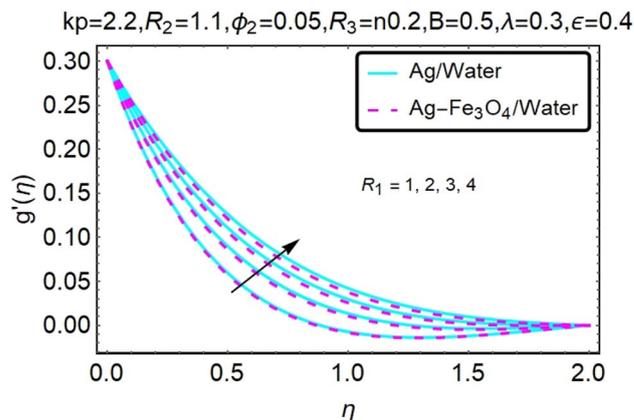

Fig. 8 Change in velocity profile by varying R_1.

Fig. 9 Change in velocity profile by varying R_1.

velocity distribution coefficient when a turn occurs. These graphs are designed to calculate flow performance based on parameters. The boundary layer thickness decreases with increasing velocity. Fig. 8 and 9 show that as velocity increases, circulation also reduces. Then we checked the performance of the velocity shape and the normal variations of the parameters involved. Changing R_1 will increase the temperature of the fluid, as shown in Fig. 8.

Stretched sheet microrotation profiles

Fig. 10–13 graphically show changes in heat transfer and flow behavior affected by several new parameters. Fig. 10–13 show the behavior of ε and k_p in the microrotation curves $h_1(\eta)$ and $h_2(\eta)$ of nanofluids (Ag/water) and mixed nanofluids (Ag-Fe$_3$O$_4$/water). Four different changes in micropolarity parameters were evaluated and the behavior of the curve in both directions was improved. At the same time, it was observed that in the case of the mixed nanofluids (Ag-Fe$_3$O$_4$/water), microrotation is very fast. Compared to simple nanofluids (Ag/water), the resistance is higher. With an increase in micropolarity parameter, except in the area near the exterior where the kinematic thickness controls the movement, rotation of the micropolar component in the boundary layer is stimulated. Fig. 10–13 show that when ε
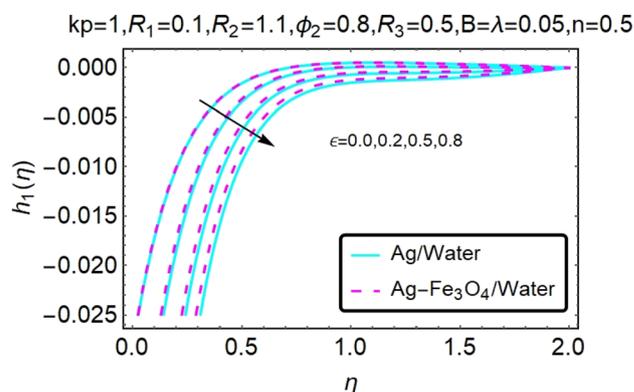

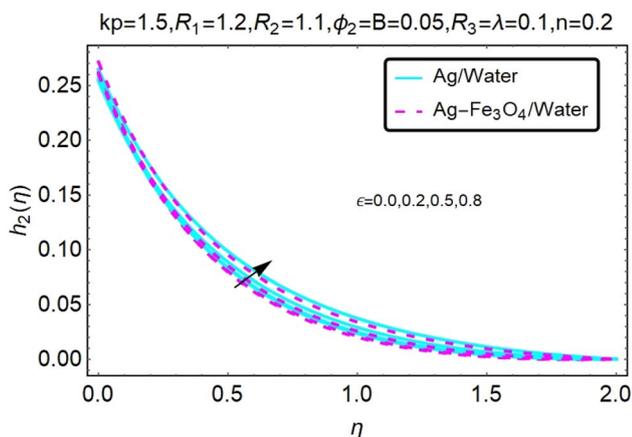Fig. 10 Change in microrotation profile by varying ε.

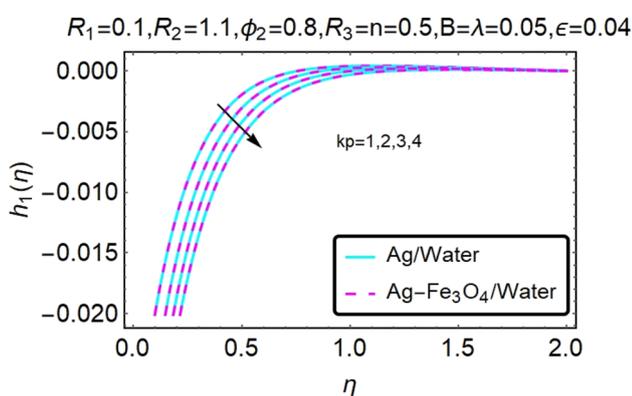**Fig. 11** Change in microrotation profile by varying ϵ.

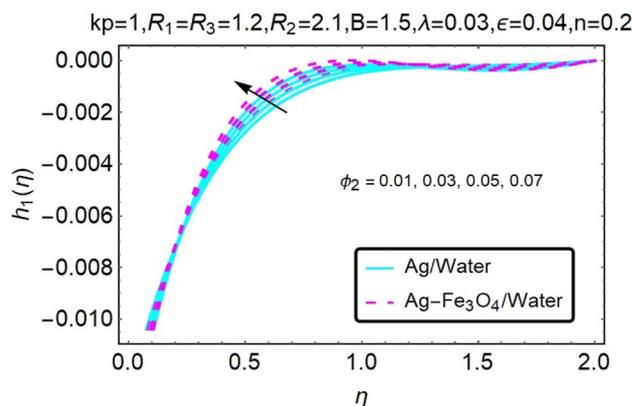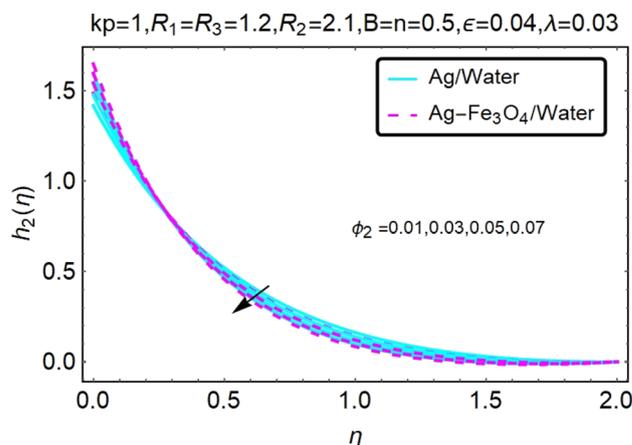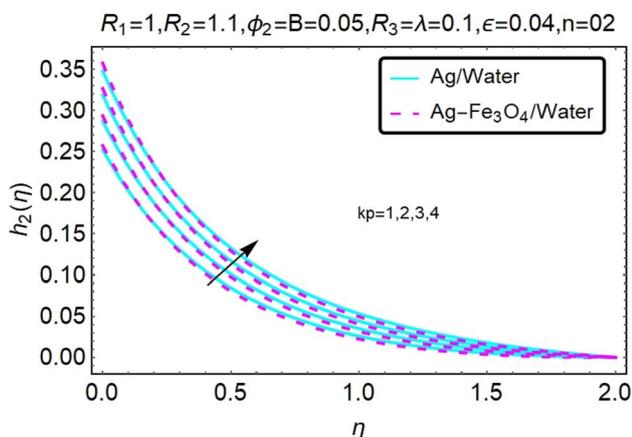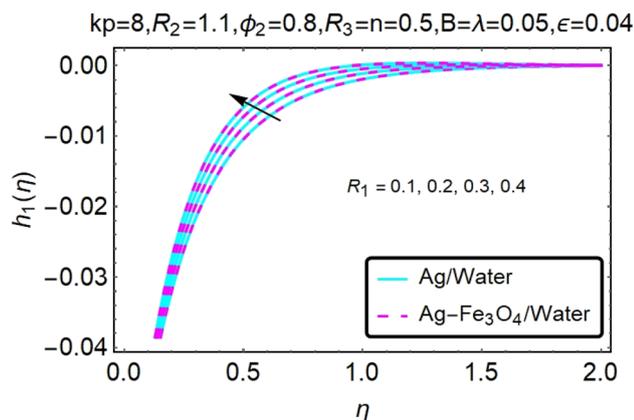**Fig. 12** Change in microrotation profile by varying k_p.

and k_p increase, the microrotation curve $h_1(\eta)$ decreases, while $h_2(\eta)$ increases.

Fig. 14 and 15 graphically show changes in heat transfer and flow behavior affected by several new parameters. Fig. 14 and 15 describe the behavior of ϕ_2 in the microrotation profiles $h_1(\eta)$ and $h_2(\eta)$ of nanofluids (Ag/water) and mixed nanofluids (Ag-
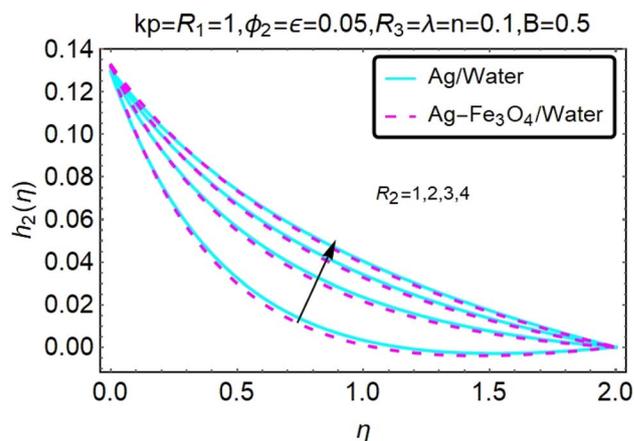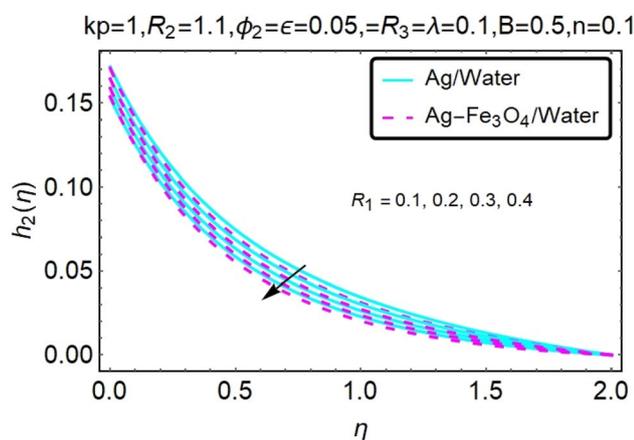

Fig. 13 Change in microrotation profile by varying k_p.
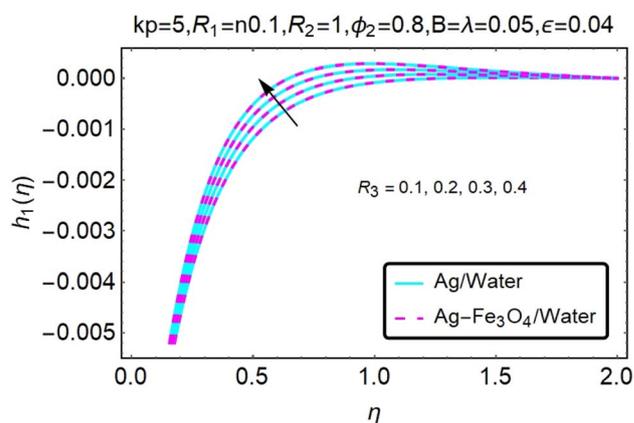

Fig. 14 Change in microrotation profile by varying ϕ_2.
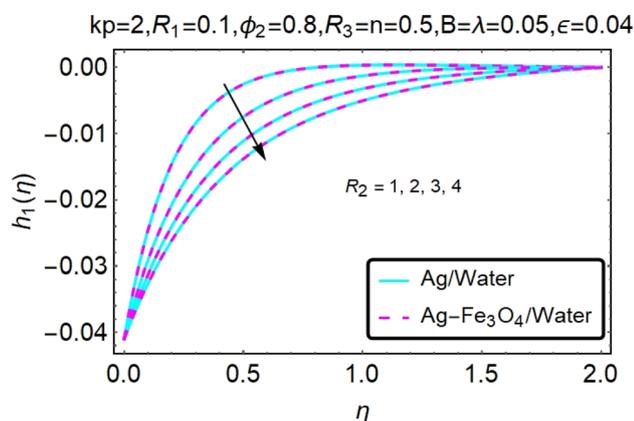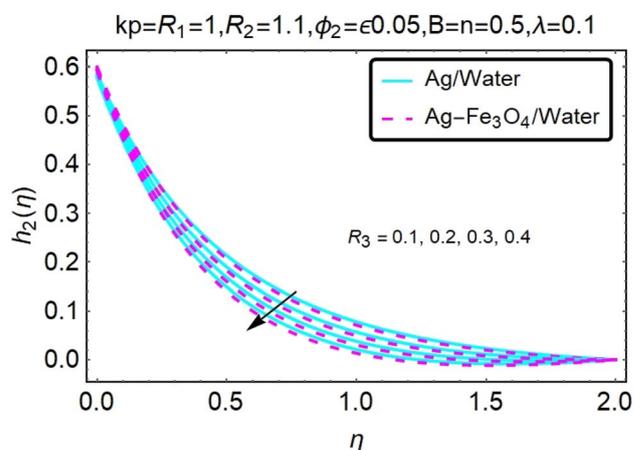

Fig. 15 Change in microrotation profile by varying ϕ_2.

Fe$_3$O$_4$/water). Four different changes in the micropolarity parameters were evaluated and an improvement in the profile behavior in two directions was recorded. At the same time, it was observed that in the case of mixed nanofluids (Ag-Fe$_3$O$_4$/water), the microrotation is very strong compared with that of simple nanofluids (Ag/water). With an increasing micropolarity parameter, except in the area near the exterior where the kinematic thickness controls the movement, rotation of the micropolar component in the boundary layer is stimulated. Fig. 14 and 15 show that when ϕ_2 increases, the microrotation profile $h_1(\eta)$ increases, while $h_2(\eta)$ decreases.

Fig. 16–21 graphically show changes in heat transfer and flow behavior affected by several new parameters. Graphs 16–21 describe the behavior of nanofluids (Ag/water) and mixed nanofluids (Ag-Fe$_3$O$_4$/water) in terms of the microrotation profiles $h_1(\eta)$ and $h_2(\eta)$ by changing R_1, R_2 and R_3. Four different changes in the micropolarity parameters were evaluated and the improvement in the profile behavior in two directions was recorded. At the same time, it was observed that in the case of mixed nanofluids (Ag-Fe$_3$O$_4$/water), the microrotation is very strong compared with that of simple nanofluids (Ag/water). With an increase in the micropolarity parameter, except in the

Fig. 16 Change in microrotation profile by varying R_1.

Fig. 17 Change in microrotation profile by varying R_1.

Fig. 19 Change in microrotation profile by varying R_2.
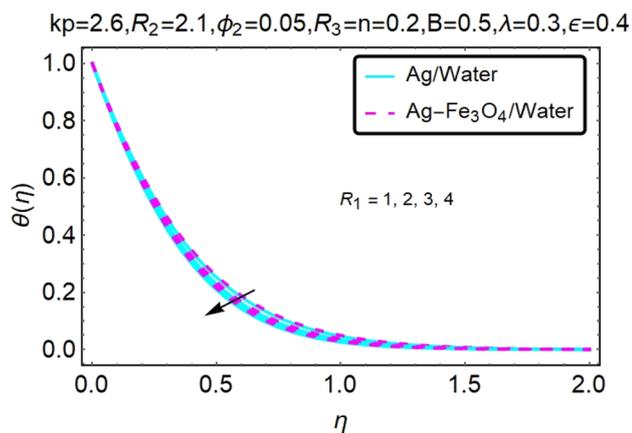

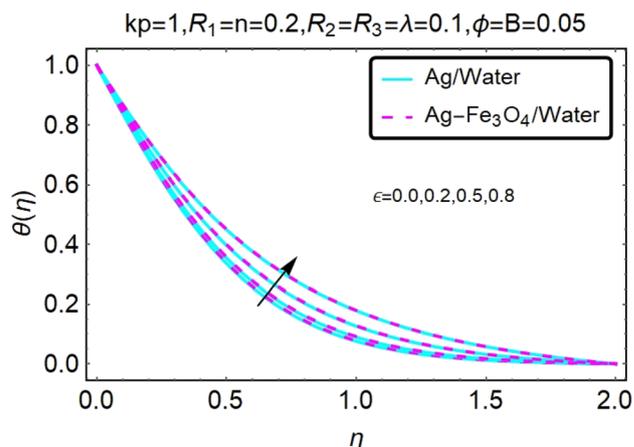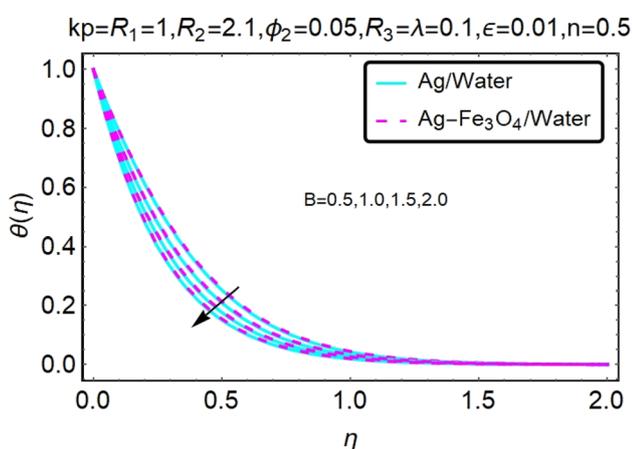**Fig. 20** Change in microrotation profile by varying R_3.

area near the exterior where the kinematic thickness controls the movement, rotation of the micropolar component in the boundary layer is stimulated. Fig. 16–21 show that when R_1, R_2 and R_3 increase, the microrotation profile $h_1(\eta)$ increases, while $h_2(\eta)$ decreases.

Stretched sheet temperature profiles

Fig. 22–26 show the results of an analysis of the temperature distribution $\theta(\eta)$ in the x and y directions, showing simple water-based fluids, nanofluids (Ag/water) and mixed nanofluids

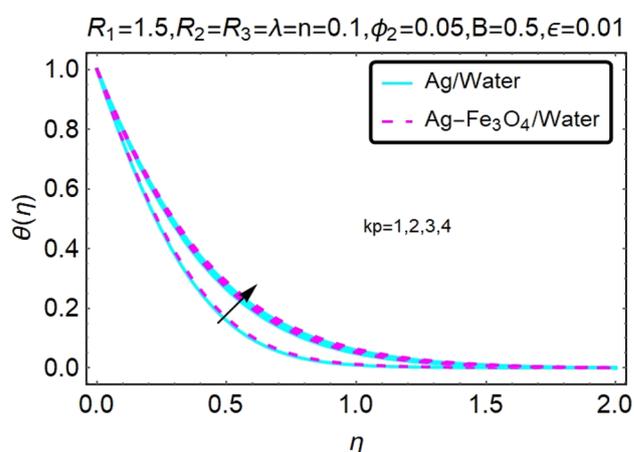**Fig. 18** Change in microrotation profile by varying R_2.

Fig. 21 Change in microrotation profile by varying R_3.

$k_p = 2.6, R_2 = 2.1, \phi_2 = 0.05, R_3 = n = 0.2, B = 0.5, \lambda = 0.3, \epsilon = 0.4$

Ag/Water
Ag–Fe$_3$O$_4$/Water

$R_1 = 1, 2, 3, 4$

Fig. 22 Change in temperature profile by varying R_1.

$k_p = R_1 = 1, R_2 = 2.1, \phi_2 = 0.05, R_3 = \lambda = 0.1, \epsilon = 0.01, n = 0.5$

Ag/Water
Ag–Fe$_3$O$_4$/Water

$B = 0.5, 1.0, 1.5, 2.0$

Fig. 23 Change in temperature profile by varying B.

Ag-Fe$_3$O$_4$/water. The difference in heat transfer and flow behavior depends on various evolution parameters, which are graphically represented in Fig. 22–26. Fig. 22–26 provide a clear description of the temperature changes when the parameters of

$k_p = 1, R_1 = R_2 = n = 0.1, R_3 = 0.2, B = 0.5, \lambda = 0.3, \epsilon = 0.4$

Ag/Water
Ag–Fe$_3$O$_4$/Water

$\phi_2 = 0.0, 0.02, 0.05, 0.08$

Fig. 24 Change in temperature profile by varying ϕ_2.

$k_p = 1, R_1 = n = 0.2, R_2 = R_3 = \lambda = 0.1, \phi = B = 0.05$

Ag/Water
Ag–Fe$_3$O$_4$/Water

$\epsilon = 0.0, 0.2, 0.5, 0.8$

Fig. 25 Change in temperature profile by varying ϵ.

$R_1 = 1.5, R_2 = R_3 = \lambda = n = 0.1, \phi_2 = 0.05, B = 0.5, \epsilon = 0.01$

Ag/Water
Ag–Fe$_3$O$_4$/Water

$k_p = 1, 2, 3, 4$

Fig. 26 Change in temperature profile by varying k_p.

the temperature relationships of R_1, B, ϕ_2, ϵ and k_p are different. The temperature increases, the relational parameters R_1, B, ϕ_2, ϵ and k_p. The effect of temperature is clearly visible. The heat rate of a mixed nanofluid is higher than that of a pure nanofluid.

$K_p = 0.7, R_1 = R_2 = n = 0.3, \epsilon = 0.4$

Ag/Water
Ag–Fe$_3$O$_4$
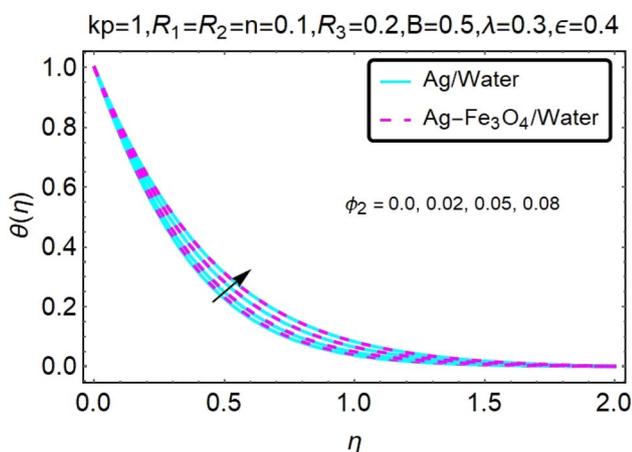
$R_3 = 0.4, 0.8, 1.2, 1.6, 2$
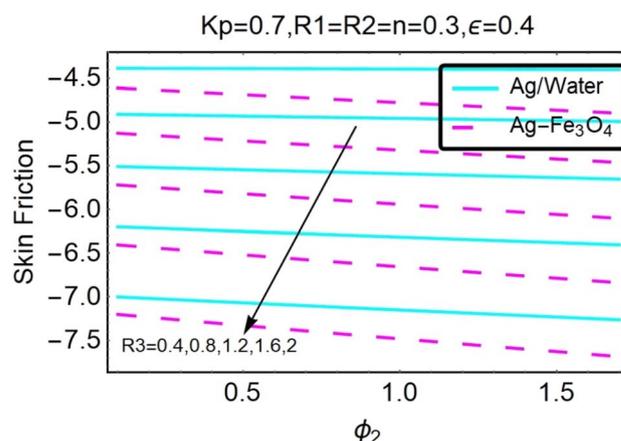
Fig. 27 The variation in skin friction for varying ϕ_2 and R_3.

When the parameters of the heat relationship between R_1, B, ϕ_2, ε and k_p change, the temperature increases.

Physical quantities

Fig. 27–30 are utilized in order to investigate the impact that varying values of form factors have on the local Nusselt number and surface friction, with each figure representing variation in a different embedded parameter. The horizontal axes are furnished with numerous values of the variable ϕ_2. According to Fig. 27, in the scenario in which the injection is coupled with a contraction, the value of the parameter R_3 raises the level of skin friction, whilst the value of the parameter ϕ_2 demonstrates the opposite behavior.

In addition to this, the nanostructures that are produced by the hybrid show excellent conductivity of heat. Plots are shown in Fig. 28 for the various values, each of which corresponds to an analysis shown in Fig. 27. Once more, research has shown that hybrid nanocomposites are superior to nanoparticles when it comes to their capacity to transport heat.

Both Fig. 29 and 30 illustrate how ϕ_2, R_3, and ε influence the pace at which heat is transferred locally. Increasing the value of
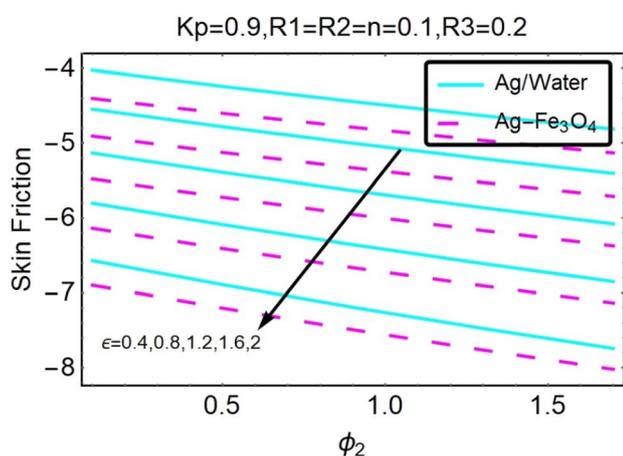

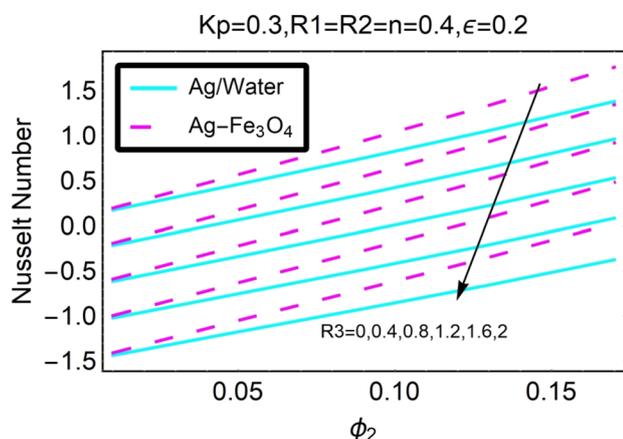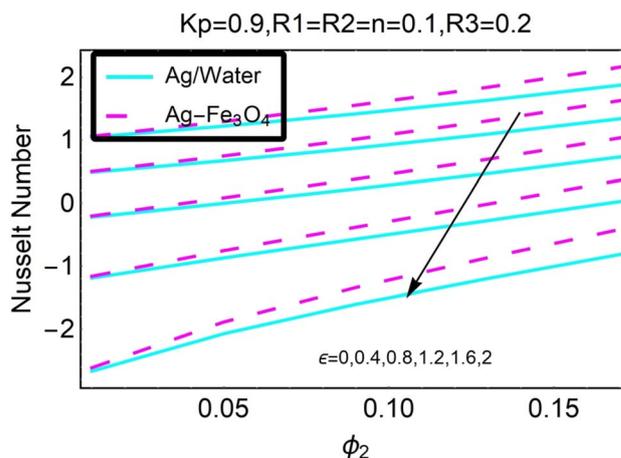**Fig. 30** The variation in Nusselt number for varying ϕ_2 and ε.

Table 4 Comparison between the present results and ref. 21

ε	R_3	Ref. 21	Current Result
0.2	0.8	4.579	4.5790
0.4		2.869	2.8691
0.6		2.321	2.3210
0.8	0.0	1.739	1.7392
	0.5	2.821	2.8211
	1.0	2.243	2.2430

Fig. 28 The variation in skin friction for varying ϕ_2 and ε.

ϕ_2 results in a decrease in the local heat transfer rates, as shown in Fig. 29. The rates for hybrid nanoparticles are significantly greater, and they are indicated against R_3 as well.

Fig. 30 illustrates the shifts that take place in the local Nusselt number as a result of an increase in its value. It has been discovered that the decreases in the local heat transfer rate caused by hybrid nanoparticles are lower than those caused by simple nanoparticles.

Table 4 presents a comparison of the outcomes of the R–K-4 approach with those of the R–K-4 method. The shooting method is also taken into consideration in this table. These two solutions appear to be totally congruent with one another. For the purposes of these calculations, the Prandtl number is assumed to be 6.2, with values of $\lambda = 0.1$, $k_p = 0.3$, and $\phi = 0.02$.

Conclusions

A computational investigation of the continuous three-dimensional boundary layer flow of a micropolar hybrid nanofluid across an exponentially stretched surface has been carried out as a result of the presence of a rotating and porous medium. In the context of this study, we conducted a qualitative comparison of nanofluids made of silver and water, as well as hybrid nanofluids made of silver, iron oxide, and water. The following is an itemized list of the most important findings from the present investigation:

Fig. 29 The variation in Nusselt number for varying ϕ_2 and R_3.

- Mixed nanofluids exhibit substantially higher heat assignment rates than simple ones.
- The temperature of the micropolar hybrid nanofluid increased even with nanoparticles of the same volume.
- The velocity distribution decreases for both the combined fluid and the individual nanofluid due to variance.
- At $n = 0$, the microrotation profiles $h_1(\eta)$ and $h_2(\eta)$ have a parabolic distribution.
- The hybrid nanofluid has a stronger effect on temperature reduction than the nanofluid due to the lower thermal conductivity of the first nanoparticle.
- As the vortex viscosity parameter R_1 increases, the velocity distributions of the mixed fluid and the nanofluid increase.
- As ϕ_2 (volume fraction), ε (rotation) and k_p (porosity parameter) increase, the speed distribution of hybrids and nanofluids is reduced.
- As the vortex viscosity parameter R_1, the spin gradient parameter R_2 and the volume fraction parameter ϕ_2 increase, the microrotation curve $h_1(\eta)$ increases and $h_2(\eta)$ decreases.
- As the rotation parameter ε, the spin gradient parameter R_2 and the porosity parameter k_p increase, the microrotation profile $h_1(\eta)$ decreases and $h_2(\eta)$ increases.

Future work

In the future, we will endeavor to expand upon this problem by incorporating ternary hybrid nanofluids with the inclusion of MHD and radiative effects.

Data availability

The datasets used and/or analyzed during the current study are available from the corresponding author on reasonable request.

Conflicts of interest

The authors declare that there is no financial/competing interest regarding this work.

Acknowledgements

References

1 N. A. Latiff, M. J. Uddin and A. M. Ismail, *Propuls. Power Res.*, 2016, **5**, 267–278.
2 U. Khan, Adnan, B. Ullah, H. A. Wahab, I. Ullah, M. A. Almuqrin and I. Khan, *Waves Random Complex Media*, 2022, pp. 1–16.
3 N. A. Amirsom, M. J. Uddin and A. I. Ismail, *Alexandria Eng. J.*, 2016, **55**, 1983–1993.
4 Adnan and W. Ashraf, *Waves Random Complex Media*, 2023, pp. 1–18.
5 B. Ullah, B. M. Fadhl, B. M. Makhdoum, K. S. Nisar and U. Khan, *Case Stud. Therm. Eng.*, 2022, **40**, 102538.
6 M. Murtaza, E. Tzirtzilakis and M. Ferdows, *Int. J. Appl. Math. Comput. Sci.*, 2018, **12**, 38–42.
7 A. Raptis, *J. Porous Media*, 2000, **3**, 95–97.
8 M. Ferdows, M. S. Khan, M. M. Alam and S. Sun, *Math. Probl. Eng.*, 2012, 1–21.
9 B. Ullah, H. A. Wahab, U. Khan and S. Bhatti, *Proc. Inst. Mech. Eng., Part E*, 2023, **237**(3), 753–761.
10 Adnan, *Waves Random Complex Media*, 2022, pp. 1–15.
11 F. Tuz Zohra, M. J. Uddin, M. F. Basir and A. I. M. Ismail, *Proc. – Inst. Mech. Eng.*, 2020, **234**, 83–97.
12 R. Rehman, U. Khan, H. A. Wahab and B. Ullah, *Waves Random Complex Media*, 2022, pp. 1–16.
13 N. K. Mishra, Adnan, G. Sarfraz, M. Z. Bani-Fwaz and S. M. Eldin, *J. Therm. Anal. Calorim.*, 2023, 1–12.
14 W. Khan, U. Khan, B. Ullah, N. Ahmed, I. Khan, A. M. Alqahtani and M. Alam, *Math. Probl. Eng.*, 2023, e202200435.
15 M. J. Uddin, N. A. Amirsom, O. A. Beg and A. I. Ismail, *Waves Random Complex Media*, 2022, 1–21.
16 Z. Zhang, J. Cui, J. Zhang, D. Liu, Z. Yu and D. Guo, *Appl. Surf. Sci.*, 2019, **467**, 5–11.
17 S. Suresh, K. P. Venkitaraj, M. S. Hameed and J. Sarangan, *J. Nanosci. Nanotechnol.*, 2014, **14**, 2563–2572.
18 M. J. Uddin, P. Rana, S. Gupta and M. N. Uddin, *Iran. J. Sci. Technol.*, 2023, 1–15.
19 M. Turkyilmazoglu, *Int. J. Non-Linear Mech.*, 2016, **83**, 59–64.
20 Adnan, *Waves Random Complex Media*, 2022, pp. 1–15.
21 M. Qadeer, M. A. Alyami, U. Khan, M. F. Yassen, S. E. Alhazmi and B. Ullah, Irreversibility analysis for flow of carbon nanotubes with varying length and radius: Applications in rocket engine, *Int. J. Mod. Phys. B*, 2023, **37**, 2350180.